Journal of Photopolymer Science and Technology
Volume 30, Number 6 (2017) 619 – 625 ©2017SPST

Controlling the Pore Structure of Polyimide Films Prepared by Exposure to High-Pressure CO_2 and UV Light

Kentaro Taki[1*], Tatsuki Isawa[2], and Akira Mizoguchi[3*]

[1] Chemical and Materials Engineering Course, School of Natural System, College of Science and Engineering, Kanazawa University, Kakumamachi, Kanazawa, Ishikawa 920-1192, Japan
**taki@se.kanazawa-u.ac.jp*
[2] Department of Natural System, Graduate School of Kanazawa University, Kakumamachi, Kanazawa, Ishikawa 920-1192, Japan
[3] Sumitomo Electric Industries, Ltd, 1-1-3, Shimaya, Konohana-ku, Osaka 554-002, Japan
**mizoguchi-akira@sei.co.jp*

Porous polyimide is a promising low-permittivity material for reducing the attenuation of high-frequency signals. Previously, the suitability of porous polyimide films for flexible printed circuits was tested by subjecting them to cover-layering and copper plating. These treatments resulted in pore collapse and infiltration, respectively, indicating the necessity of using closed-pore films. Herein, closed-pore porous polyimide films were prepared at various CO_2 gas pressures, tertiary amine methacrylate monomer concentrations, and pre-baking times, revealing the key role of pre-baking time in maximizing porosity while preserving closed pores. In contrast to our previous study, the formation of closed pores was explained by a novel mechanism featuring CO_2 bubble nucleation as a key step.
Keywords: Closed pore, Foaming, Porosity, Bubble nucleation, Dielectric constant

1. Introduction

The inherently high heat resistance, flexibility, and chemical stability of polyimide (PI) films account for their widespread utilization in the electronics industry to produce flexible printed circuits (FPCs). However, the increasing demand for mobile devices capable of faster data transfer requires the use of PI FPCs with low dielectric constants to decrease signal attenuation. Therefore, dielectric constant reduction has been investigated by several researchers, as summarized in prior studies [1,2] and reviews [3,4] and in our previous articles [5,6].

The introduction of 10-nm pores into PI for applications such as integrated circuit insulators was pioneered by Hedrick [7], who designed a block copolymer system that could be pyrolyzed at high temperatures to successfully form voids in the PI matrix. However, the small number of produced pores resulted in low porosity. Another approach to forming pores involves physical foaming, featuring thermal phase-separation of CO_2 gas dissolved in a polymer matrix to induce bubble nucleation in the glassy and rubbery polymer state [8,9]. This method allows dielectric constants as low as 1.77 to be achieved, corresponding to an ultralow-k level [9]. Mesoscale domains in the PI matrix can be removed by supercritical fluid–assisted extraction, with the remaining domains allowed to become voids [10]. This concept was further examined for poly(methyl methacrylate) and polystyrene [11]. Although the process of mesopore formation is highly sophisticated, complete extraction of all domains is considered to be impossible, hindering the application of such materials in electronic devices. As an alternative, waterborne porous PI has been prepared via condensation of water vapor onto a PI solution spun on a substrate [2], with micron-sized condensed water droplets acting as a porogen. This method allows the dielectric constant of porous films to be further reduced to 1.7, although a 48-h

Received May 16, 2017
Accepted June 30, 2017

time period was required for water droplets to form in these porous films, with other porogens also extensively studied [12-23].

Recently, we have discovered a system suitable for generating ultralow-k PI films of high porosity using a short processing step [24]. Figure 1 shows the mechanism of porous PI film formation from poly(amic acid) (PAA) solution, CO_2, and a UV-curable *tert*-amine monomer, with a mixture of PI precursor, solvent, and UV-curable monomer/photoinitiator used as a negative-tone PI resist. The monomer and solvent were dispersed in PAA solution after vaporizing a certain amount of solvent. The subsequently introduced high-pressure CO_2 reacted with the monomer to form zwitterionic salts, resulting in immediate phase separation and the formation of solvent droplets in domains surrounded by the above salts. Next, polymerization of monomers in an atmosphere of high-pressure CO_2 was induced by UV light irradiation, solidifying the transient structure of the phase-separated mixture featuring droplets in wet film. After the CO_2 pressure was decreased, the solvent droplets vaporized to form pores, with the whole pore formation and solidification process being complete within 2 min. The thus obtained porous PI precursor was converted into porous PI by thermal treatment.

In our previous study, we tested the suitability of porous polyimide films for flexible printed circuits by subjecting them to cover-layering and copper plating [6]. The results showed that cover-layering induced the collapse of some pores, with copper plating leading to pore infiltration, indicating that such treatments require closed-pore films. Herein, CO_2 gas pressure, monomer (tertiary amine

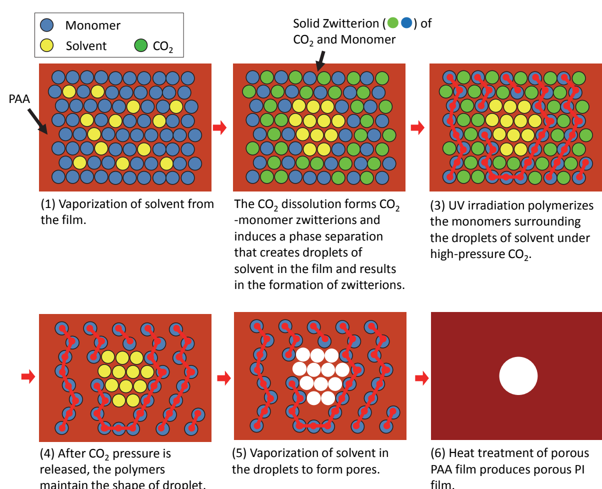

Fig. 1. Mechanism of pore formation in PI films [24].

methacrylate) concentration, and pre-baking time were varied to prepare closed-pore porous polyimide films.

2. Experimental

2.1. Materials

Poly(amic acid) (PAA) solution was prepared by polymerization of pyromellitic dianhydride and 4,4'-diaminodiphenyl ether in *N*,*N*-dimethyl acetamide at 80 °C under nitrogen, with solid content of the solution equaling 15 wt%.

To prepare the standard formulation (denoted in previous studies [5,24]), 1.58 g (8.53 mmol) of UV-curable 2-(diethylamino)ethyl methacrylate monomer (DEMA; TCI, Japan) and 0.201 g (0.577 mmol) of diphenyl(2,4,6-trimethylbenzoyl) phosphine oxide (photoinitiator; Irgacure TPO, BASF) were added to 6.56 g of the PAA solution and stirred until a homogeneous solution was obtained. To clarify the effect of monomer concentration on pore structure, the monomer concentration was reduced from that used in the standard formulation.

2.2. UV light exposure in high-pressure CO_2

Porous polyimide films were prepared utilizing UV light irradiation in high-pressure CO_2, as reported in previous studies [7,8].

A 200-μm-gap baker film applicator was used to cast the PAA solution on a smooth copper foil placed on a hot-plate held at 40 °C at a rate of 30 mm/s. The pre-baking was performed on the hot-plate at 40°C for a given pre-baking time.

The above foil was placed into a high-pressure CO_2 UV light exposure apparatus, with the CO_2 dissolution time and pressure equaling 60 s and 6.5 MPa, respectively, and UV light exposure time and intensity at 365 nm equaling 60 s and 80% of maximum intensity (~200 mW/cm^2), respectively.

Conversion of the precursor into porous PI film was achieved by thermal treatment in a nitrogen-flushed oven (DN610I, Yamato Scientific, Tokyo, Japan) using the following temperature gradient: (1) 40 °C for 120 min, (2) 3 °C/min to 110 °C for 60 min, and (3) 3 °C/min to 320 °C for 60 min under 20 L/min of nitrogen.

2.3. Characterization of porous PI

Cross-sectioned samples were obtained using an Ar ion beam cross-section polisher (IB-09020CP, JEOL, Japan), typically employing an acceleration voltage of 6.0 kV, an emission current of 180 μA, and an operation time of 5 h. The obtained samples

were observed by field emission scanning electron microscopy (SEM; Ultra55, Carl Zeiss, Germany) without any metal coating. A low acceleration voltage of 1 kV was used to avoid charge-up, with the working distance equaling 5 mm.

3. Results and discussion

The abovementioned mechanism of porous PI film formation features the key reaction of CO_2 with the tertiary amine to produce zwitterions. To control the amount of produced zwitterions and thus the pore structure of the film, the amounts of CO_2 and tertiary amine were varied independently.

3.1. CO_2 pressure

CO_2 reacts with the tertiary amine monomer to form zwitterions that induce the formation of solvent droplets. Therefore, the effect of CO_2 pressure (which controls the CO_2 concentration in solution) on pore structure was investigated for a range of 4.5–6.5 MPa, with the monomer concentration and pre-baking time equaling 19 wt % and 5 min, respectively.

The effect of CO_2 pressure on pore structure is illustrated in Fig. 2, which depicts film cross-sections where pores are shown as dark ellipsoidal areas. The film produced under standard conditions (6.5 MPa CO_2 pressure, 19 wt% monomer content, and 5 min baking time) is shown in Fig. 2-(d), revealing that decreased CO_2 pressure results in a reduced number of pores. However, the pores produced at a reduced pressure of 4.5 MPa were still interconnected, showing that the reduction of CO_2 pressure can effectively reduce the number and size of pores while preserving their interconnected nature.

3.2. Monomer concentration

Monomer concentration is the key factor influencing zwitterion and solvent drop formation, with its effect on pore structure shown in Fig. 3. In this test, the monomer concentration was stepwise reduced from 19 wt% (Fig. 2-(d)) to 7 wt%, revealing that the pore size decreased upon reducing the monomer concentration from 19 to 7 wt%, increased upon further reduction to 9 wt%, and finally decreased at a concentration of 7 wt%. The film obtained at a concentration of 11 wt% showed higher porosity than that observed for the standard formulation (19 wt%), with some pores being still connected. The distinctive porous structure of the 7 wt%-sample featured pores that were collapsed and elongated in the horizontal

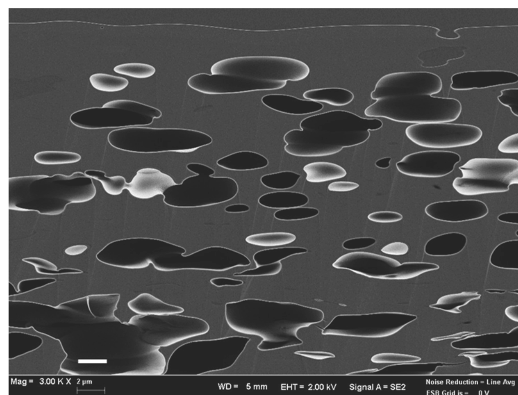

(a) 4.5 MPa CO_2.

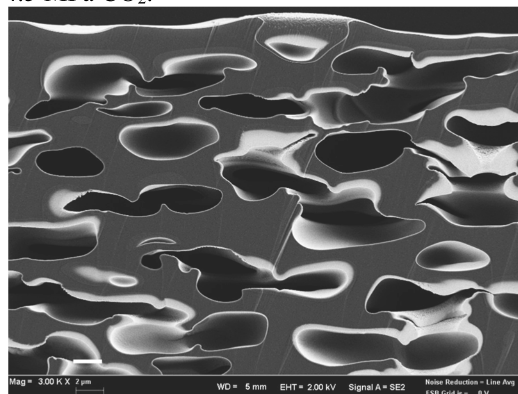

(b) 5.0 MPa CO_2.

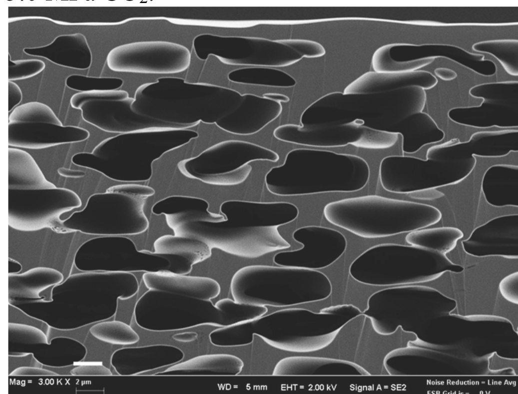

(c) 6.0 MPa CO_2.

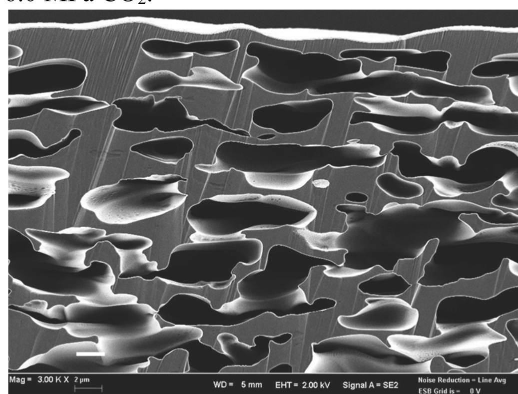

(d) 6.5 MPa CO_2.

Fig. 2. Cross-sectional SEM images of films obtained at CO_2 pressures of (a) 4.5, (b) 5.0, (c) 6.0, and (d) 6.5 MPa. Scale bar = 2 μm.

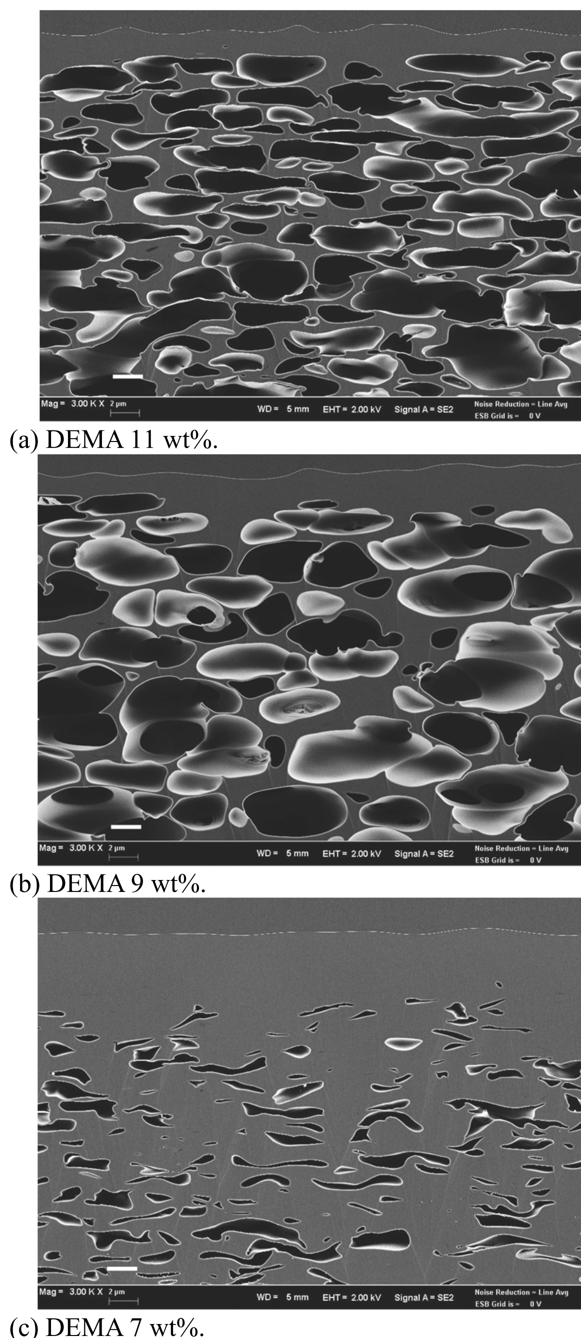

(a) DEMA 11 wt%.

(b) DEMA 9 wt%.

(c) DEMA 7 wt%.

Fig. 3. Effect of monomer concentration on pore structure: (a) 11, (b) 9, (c) 7 wt%. Scale bar = 2 μm.

direction. Although most of these pores were isolated, the observed porosity was too low for a practically applicable low-dielectric-constant film.

Thus, although monomer concentration reduction can effectively reduce the number of pores, there is no optimal concentration for simultaneously realizing high porosity and isolated (closed) pores.

3.3. Pre-baking time

To control the amount of solvent in the film, pre-baking times of 1, 3, 5, 7, 10, 50, 100, and 200 min were used, with the CO_2 pressure and monomer concentration kept at 6.5 MPa and 19 wt %, respectively.

The effect of pre-baking time on pore structure is shown in Fig. 4, revealing that interconnected pores were obtained at times of 1 to 7 min. Notably, collapsed and heterogeneously interconnected pores were observed at a time of 1 min, and the largest film thickness was observed in the case of 7 min. When the CO_2 pressure was reduced from 6.5 MPa to ambient values to open the pressure chamber and remove the sample after UV light irradiation, CO_2 bubbles were produced in and on the film, with some bubbles inducing blister formation and thus significantly damaging the film surface. However, almost no blisters were formed as the pre-baking time was further increased.

At a time of 10 min, isolated pores and relatively high porosity were observed, and the pore structure was remarkably changed. There is a skin layer where pores do not exist in top of 1/3 thickness. The number of pores in a view of SEM micrograph decreased as pre-baking time was increased further, e.g., 5 pores were formed in the case of 100 min and 6 pores in the case of 200 min, with their size equaling ~2–4 μm.

The dramatic pore structure change observed at increased pre-baking times could be explained by skin layer formation. At times between 1 and 7 min, no distinctive skin layer was formed. However, at 10 min, a skin layer with interconnected pores was detected, with these pores becoming isolated in the case of longer pre-baking times (50, 100, and 200 min).

Pre-baking is required for vaporizing the solvent from the film, i.e., for film drying, with the drying rate governed by mass and heat transfer at the air/film interface. Initially, a constant drying rate period was observed, followed by a decrease of the drying rate due to rate-determined phenomena is changed to mass transfer of solvent in film with decreasing the solvent concentration. At some point, a vertical concentration gradient appeared in the film, marking the onset of the falling rate period [25].

Typical drying phenomena occurring at pre-baking times of 1–7 min correspond to the constant drying rate period, characterized by the absence of a solvent concentration gradient, uniform solvent vaporization, and, therefore, uniformly distributed pores. This scenario was assumed for pore formation by zwitterion-induced phase separation and subsequent solvent droplet

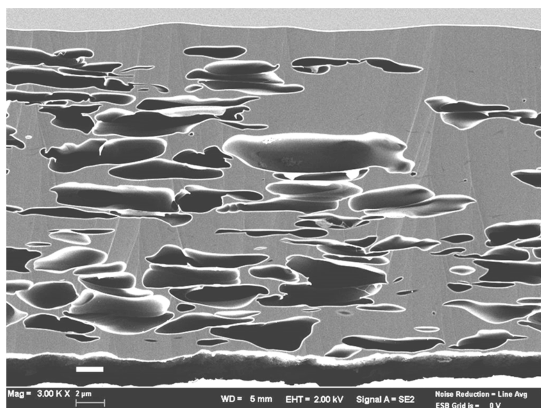

(a) 1 min.

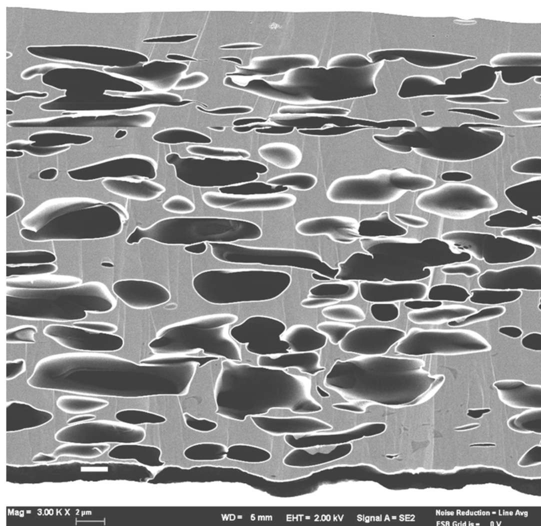

(b) 3 min.

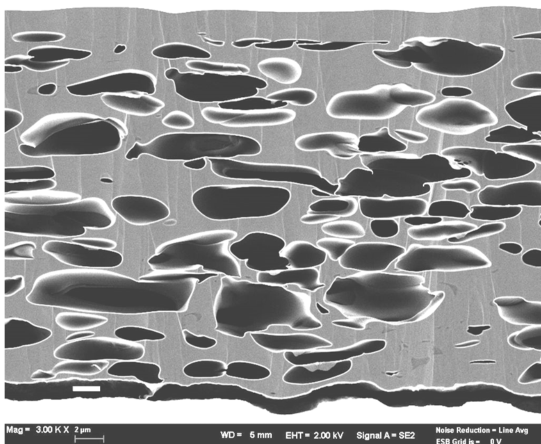

(c) 5 min.

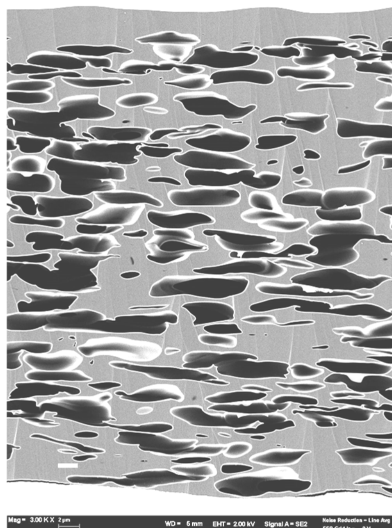

(d) 7 min.

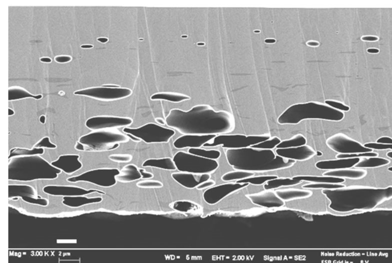

(e) 10 min.

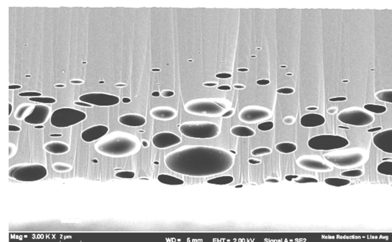

(f) 50 min.

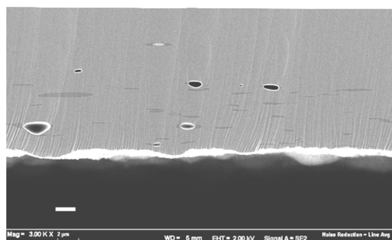

(g) 100 min.

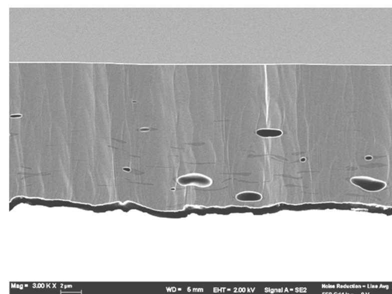

(h) 200 min.

Fig. 4. Effect of pre-baking time on pore structure. Scale bar = 2 µm.

formation.

The effect of pre-baking time on pore structure is shown in Fig. 4, revealing that interconnected pores were obtained at times of 1 to 7 min. Notably, collapsed and heterogeneously interconnected pores were observed at a time of 1 min, and the largest film thickness was observed in the case of 7 min. When the CO_2 pressure was reduced from 6.5 MPa to ambient values to open the pressure chamber and remove the sample after UV light irradiation, CO_2 bubbles were produced in and on the film, with some bubbles inducing blister formation and thus significantly damaging the film surface. However, almost no blisters were formed as the pre-baking time was further increased.

At a time of 10 min, isolated pores and relatively high porosity were observed, and the pore structure was remarkably changed. There is a skin layer where pores do not exist in top of 1/3 thickness. The number of pores in a view of SEM micrograph decreased as pre-baking time was increased further, e.g., 5 pores were formed in the case of 100 min and 6 pores in the case of 200 min, with their size equaling ~2–4 μm.

The dramatic pore structure change observed at increased pre-baking times could be explained by skin layer formation. At times between 1 and 7 min, no distinctive skin layer was formed. However, at 10 min, a skin layer with interconnected pores was detected, with these pores becoming isolated in the case of longer pre-baking times (50, 100, and 200 min).

Pre-baking is required for vaporizing the solvent from the film, i.e., for film drying, with the drying rate governed by mass and heat transfer at the air/film interface. Initially, a constant drying rate period was observed, followed by a decrease of the drying rate due to rate-determined phenomena is changed to mass transfer of solvent in film with decreasing the solvent concentration. At some point, a vertical concentration gradient appeared in the film, marking the onset of the falling rate period [25].

Typical drying phenomena occurring at pre-baking times of 1–7 min correspond to the constant drying rate period, characterized by the absence of a solvent concentration gradient, uniform solvent vaporization, and, therefore, uniformly distributed pores. This scenario was assumed for pore formation by zwitterion-induced phase separation and subsequent solvent droplet formation.

The pre-baking time of 10 min corresponds to the transition between constant drying and falling rate periods, and times of 50–200 min correspond to the falling rate period, characterized by the existence of a solvent concentration gradient and reduced solvent amount. The solvent droplet produced by the zwitterion was no longer existed. The most of solvent “dissolved” in the area where the solvent droplet existed. Under these conditions, pores were supposed to form by CO_2 bubble nucleation and grow as the CO_2 pressure was reduced, thus exhibiting an isolated and closed character.

The obtained results are summarized in Table 1, with each porous structure scored from the viewpoint of open/closed pore nature (i.e., interconnected or isolated pores) and porosity. The following ranking system was used: one star (*) corresponds to films with open pores that are unsuitable for FPC applications; two stars (**) correspond to films with closed pores but low porosity that are therefore ineffective for the above applications; finally, three stars (***) corresponds to films with closed pores and high porosity that are suitable for the above application films. As shown in Table 1, the three-star (***) rating was given to films obtained under the experimental conditions of Fig. 4-(f), corresponding to CO_2 pressure, monomer concentration, and pre-baking time of 6.5 MPa, 19%, and 50 min, respectively.

Table 1. Effects of CO_2 pressure, monomer concentration, and pre-baking time on pore structure.

Fig.	CO_2	DEMA	Pre-baking time	Score
-	MPa	%	min	-
2-a	4.5	19	5	*
2-b	5.0	19	5	*
2-c	6.0	19	5	*
2-d	6.5	19	5	*
3-a	6.5	11	5	*
3-b	6.5	9	5	*
3-c	6.5	7	5	**
4-a	6.5	19	1	*
5-b	6.5	19	3	*
4-c	6.5	19	5	*
4-d	6.5	19	7	*
4-e	6.5	19	10	*
4-f	6.5	19	50	***
4-g	6.5	19	100	**
4-h	6.5	19	200	**

*Open pores. **Closed pores, low porosity. ***Closed pores, high porosity.

4. Conclusion

This study elucidated optimal experimental conditions for forming PI films with closed pores and relatively high porosity, corresponding to CO_2 pressure, monomer concentration, and pre-baking time of 6.5 MPa, 19%, and 50 min, respectively. The pore formation mechanism was different from the previously proposed one at pre-baking times above 10 min, which corresponded to the falling rate period characterized by skin layer formation and CO_2 bubble nucleation. The produced CO_2 bubbles formed closed and isolated pores, resulting in films suitable for low-dielectric-constant FPC applications.

Acknowledgements

This study was supported by the Grant-In-Aid of Japanese government for Challenging Exploratory Research (16K14469) and the New Energy and Industrial Technology Development Organization, Japan (NEDO, 09A16003d). We would like to thank Editage (www.editage.jp) for providing English language editing service.

References

1. M. H. Weng, H. W. Wu, Y. K. Su, R. Y. Yang, and C. Y. Hung, *Microw. Opt. Technol. Lett.*, **48** (2006) 1675.
2. Y. Ren and D. C. C. Lam, *J. Electron. Mater.*, **37** (2008) 955.
3. X.-Y. Zhao and H.-J. Liu, *Polym. Int.*, **59** (2010) 597.
4. S. Ma, Y. Wang, Z. Min, and L. Zhong, *Adv. Polym. Technol.*, **32** (2013) 21358.
5. K. Taki and H. Ito, *J. Photopolym. Sci. Technol.*, **28** (2015) 747.
6. K. Taki, A. Mizoguchi, and H. Ito, *J. Photopolym. Sci. Technol.*, **29** (2016) 459.
7. J. L. Hedrick, R. D. Miller, C. J. Hawker, K. R. Carter, W. Volksen, D. Y. Yoon, and M. Trollsas, *Adv. Mater.*, **10** (1998) 1049.
8. B. Krause, K. Diekmann, N. F. A. van der Vegt, and M. Wessling, *Macromolecules*, **35** (2002) 1738.
9. B. Krause, G. H. Koops, N. F. A. van der Vegt, M. Wessling, M. Wubbenhorst, and J. van Turnhout, *Adv. Mater.*, **14** (2002) 1041.
10. A. Mochizuki, T. Fukuoka, M. Kanada, N. Kinjou, and T. Yamamoto, *J. Photopolym. Sci. Technol.*, **15** (2002) 159.
11. F. Lv, L. Liu, Y. Zhang, and P. Li, *J. Appl. Polym. Sci.*, **132** (2015) 41480.
12. Y. J. Lee, J. M. Huang, S. W. Kuo, and F. C. Chang, *Polymer*, **46** (2005) 10056.
13. Y. J. Lee, J. M. Huang, S. W. Kuo, J. S. Lu, and F. C. Chang, *Polymer*, **46** (2005) 173.
14. J. J. Lin and X. D. Wang, *Polymer*, **48** (2007) 318.
15. M. A. Wahab, K. Y. Mya, and C. B. He, *J. Polym. Sci., Part A: Polym. Chem.*, **46** (2008) 5887.
16. Z. M. Dang, L. J. Ma, J. W. Zha, S. H. Yao, D. Xie, Q. Chen, and X. Duan, *J. Appl. Phys.*, **105** (2009) 044104.
17. G. F. Zhao, T. Ishizaka, H. Kasai, M. Hasegawa, T. Furukawa, H. Nakanishi, and H. Oikawa, *Chem. Mater.*, **21** (2009) 419.
18. A. Bittner, H. Seidel, and U. Schmid, *Microelectron. Eng.*, **88** (2011) 2977.
19. J. Im, S. Y. Hong, Y. Cheon, J. Lee, J. S. Lee, H. S. Kim, M. Cheong, and H. Park, *Energy Environ. Sci.*, **4** (2011) 4284.
20. Y. X. Jin, J. Tang, J. Hu, X. Han, Y. Z. Shang, and H. L. Liu, *Colloids Surf. A*, **392** (2011) 178.
21. S. Devaraju, M. R. Vengatesan, M. Selvi, A. A. Kumar, and M. Alagar, *High Perform. Polym.*, **24** (2012) 85.
22. S. Chisca, I. Sava, and M. Bruma, *Polym. Int.*, **62** (2013) 1634.
23. S. S. Park and C. S. Ha, *Compos. Interfaces*, **23** (2016) 831.
24. K. Taki, K. Hosokawa, S. Takagi, H. Mabuchi, and M. Ohshima, *Macromolecules*, **46** (2013) 2275.
25. D. I. Onwude, N. Hashim, R. B. Janius, N. M. Nawi, and K. Abdan, *Compr. Rev. Food Sci. Food Saf.*, **15** (2016) 599.